OPEN ACCESS

An Insight into the Mechanisms of Energy Storage in a Double Layer Capacitor with ILs and a Microporous Carbon: Experimental Evidences of Ion-Swapping by Electrochemical Impedance Spectroscopy

To cite this article: Noemí Quintanal *et al* 2023 *J. Electrochem. Soc.* **170** 040528

Journal of The Electrochemical Society, 2023 **170** 040528

An Insight into the Mechanisms of Energy Storage in a Double Layer Capacitor with ILs and a Microporous Carbon: Experimental Evidences of Ion-Swapping by Electrochemical Impedance Spectroscopy

Noemí Quintanal, Daniel Barreda, Clara Blanco, Zoraida González, Patricia Álvarez, Marcos Granda, Marta Sevilla, and Ricardo Santamaría[z]

Instituto de Ciencia y Tecnología del Carbono (INCAR), CSIC, Francisco Pintado Fe 26, 33011 Oviedo, Spain

The energy storage mechanism operating in carbon-based supercapacitors using ionic liquids as electrolytes is not yet fully understood. In this paper, the interactions of ions of two widely used ionic liquids, i.e. EMImTFSI and $EMImBF_4$, with a high specific surface area microporous carbon are investigated. Galvanostatic cycling experiments performed on each electrode and in the full cell demonstrate that a specific energy close to 46 Wh kg^{-1} can be achieved with this carbon. More interestingly, impedance spectroscopy studies reveal the presence of some unusual behavior, such as the presence of inductive elements in some of the electrodes, either in the positive or in the negative electrode. These inductive elements are identified, for the first time, as another type of possible experimental evidences of some phenomena previously proposed, such as ion-swapping or co-ions desorption, both phenomena leading to the formation of the superionic state.

 [DOI: 10.1149/1945-7111/acce73]

Manuscript submitted February 13, 2023; revised manuscript received April 14, 2023. Published April 27, 2023.

Supplementary material for this article is available online

Electrochemical double layer capacitors store energy at the electrolyte–electrode interface through the reversible ion adsorption onto the electrode surface (mainly carbon materials).[1] This double-layer capacitance, firstly defined by Helmholtz (1879)[2] and later refined by Gouy[3,4] & Chapman,[5] and Stern & Geary,[6] forms due to the electrostatic attraction between the polarized electrode and the counter-ions of the electrolyte.

Although the concept of double-layer helps to easily understand how energy is stored in a supercapacitor, it also creates a rather simplistic image of the processes involved in the nanoscale. This is especially true when the double-layer is not formed on a flat surface, but in a complex surface made up of pores of similar size to that of the ions that form the double-layer, creating a nanoconfined environment. Even more complexity is added when the electrolyte used to form the double-layer is an ionic liquid (IL). The large size of the ions —often similar to the size of the pores—, the strong interaction of the ions due to the lack of solvent, the very high concentration of ions and the complex interactions developed between the ions themselves and with the surface, greatly complicates the full description of the processes involved in the energy storage.

The conventional route to increase the specific energy of supercapacitors, while maintaining power and cyclability, is to modify the carbon materials in the electrodes to increase the double-layer capacitance, adapting the porous network to the electrolyte ions. The initial belief was that the best pore sizes for ion storage were those of around double size that of solvated ions, which led to the development of mesoporous carbons with very narrow pore size distributions.[7,8] A very interesting finding was made by Chmiola et al. in 2006 by using carbide derived carbons (CDCs) with pore sizes tunable with sub-angstrom accuracy.[9] They, unexpectedly, demonstrated that pores smaller than the size of solvated ions were accessible and produced a significant increase in the double-layer capacitance. The proposed hypothesis to explain this unexpected result is the distortion of the ion solvation shell and the partial desolvation of the ions, which enables the ions to access pores of a size equal to or slightly larger than the size of the bare ion, reducing, therefore, the double-layer thickness and consequently improving the capacitance.

Several interesting studies, mainly based on theoretical calculations, followed the discoveries of Chmiola et al. trying to explain and optimize the increase in double-layer capacitance. Most of these studies were performed using ionic liquids. These electrolytes allow working at higher potentials and have the singularity that they do not need a solvent, which allows obtaining higher ion densities within the pores. In 2012 Kondrat et al. presented an excellent work based in Monte Carlo simulations where they showed the existence of a "superionic state."[10] This superionic state is reached as a consequence of the interactions between the conductive surface of the pores and the counter ions of the electrolyte that weaken the attractive forces between the IL ions. This allows the packing of higher densities of counterions within the pore, increasing thereby the specific energy. Initially, the pores are filled with both the counterions and co-ions. As the voltage increases, the electric field forces the co-ions to leave the cavity and to be substituted by more counterions (ion swapping). At even higher voltages, larger amounts of counterions can be pushed into the pores, reaching the superionic state.

Other investigations have provided similar results,[11–15] but more experimental evidences are still needed in the scientific literature beyond the unexpected increase of capacitance for materials with small pore size. The calculations of normalized double-layer capacitance (i.e., capacitance per unit of specific surface area) have to be taken with caution as the "surface area" involved in the double-layer formation cannot be directly measured. Gas adsorption experiments are normally used to calculate the specific surface area of the electrode material. But the experimental conditions of such experiments (high vacuum, etc.) and the mathematical models required to transform the gas adsorption into specific surface area values might be very far from the solid/liquid interface that exists in an EDLC when the surface is polarized and the double-layer is formed.

The aim of this study is to further understand the parameters that influence the formation of the double-layer when carbon materials are used as electrodes and ILs as electrolytes. To achieve this goal, two different ILs are used to interact with a chemically activated carbon, and a detailed electrochemical study is performed using

[z]E-mail: riqui@incar.csic.es

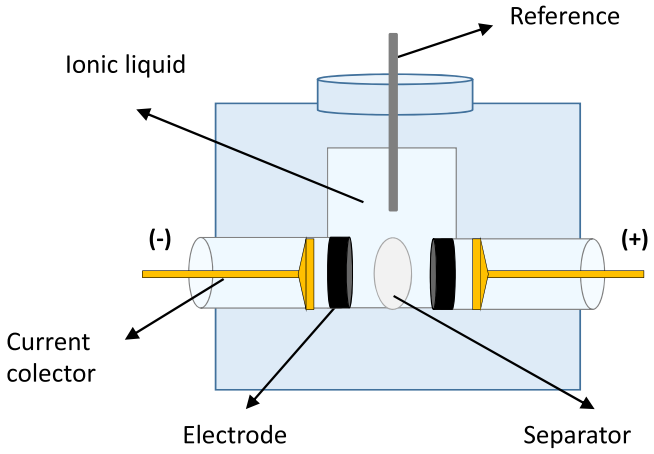

Figure 1. Scheme of a symmetric cell assembled in a two-three electrode configuration.

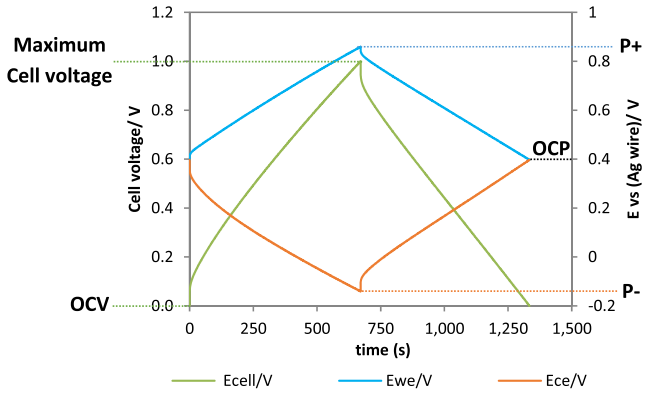

Figure 2. Galvanostatic charge- discharge profile scheme at operating cell voltage (left *Y*-axis) and potential profiles for the positive and negative electrodes (right *Y*-axis).

simple symmetrical cells. This kind of carbons can develop, depending on the activation conditions, very high specific surface areas with relatively narrow micropores size distributions and have demonstrated their excellent performance in aqueous electrolytes.[16–21] The main electrochemical tool used herein is the synchronous chronoamperometric test, a technique that allows the simultaneous recording of cell voltage and electrode potentials windows (vs reference electrode) and, thereby, allows the study of simultaneous processes occurring in the positive and negative electrodes in a real cell during charge and discharge. The use of impedance spectroscopy yielded some very interesting results that gave novel experimental proofs of the possible existence of the superionic state or ion-swapping, that has been proposed in several investigations discussed previously. The authors believe that the presence of inductive phenomena in some electrode materials can be explained as a result of the removal of co-ions from the small nanopores during the formation of the superionic state.

Experimental

Materials.—An activated carbon (AC, $S_{BET} \approx 2200\ m^2\ g^{-1}$) was employed as active electrode material. This was synthesized in the laboratory by chemical activation of a mesophase pitch (derived from a byproduct from the carbochemical industry) with KOH. Briefly, the mesophase pitch was mixed with the activation agent in a proportion 3:1 (KOH/pitch) in a mortar. Then, the sample was carbonized at 700 °C for 1 h, under a N_2 flow. Afterwards, the activated sample was washed with a 3 M HCl solution to remove the inorganic species and finally with distilled water until neutral pH was achieved. The AC thus obtained, labeled as AC3:1, was dried in a vacuum oven at 100 °C for 24 h.

Two ionic liquids (ILs) were used as electrolyte: 1-Ethyl-3-methylimidazolium bis(trifluoromethylsulfonyl)imide (EMImTFSI, Sigma-Aldrich, ⩾98% purity, with ⩽0.5% water, Germany) and 1-Ethyl-3-methylimidazolium tetrafluoroborate (EMImBF$_4$, Sigma-Aldrich, ⩾98% purity, with ⩽0.5% water, Germany).

Structural characterization.—N_2 physisorption experiments have been carried out on a Micromeritics apparatus (ASAP 2020) at −196 °C. Before each measurement, the samples were degassed under vacuum at 150 °C for 1 h. Specific surface areas have been calculated from the N_2 physisorption measurements using the BET-method, for which an appropriate relative pressure range was selected to ensure a positive line intersect of multipoint BET fitting ($C > 0$). Pore volumes and pore size distributions have been calculated from the adsorption branch of the N_2 isotherms using the quenched solid density functional theory (QSDFT) for N_2 on carbon, assuming slit-shaped pores. Post-mortem analyses were performed by means of SEM measurements on randomly selected areas of used electrodes (after 10 cycles of charge/discharge by GCPL at selected voltages) using a Quanta FEG650 (FEI) instrument fitted with an EDX (Ametek-EDAX) to allow the detection and quantification of the fluorine present in selected areas.

Electrochemical characterization.—The electrodes were prepared (without adding any conductive additive) by mixing 90% by weight of the active carbon material and 10% by weight of polytetrafluoroethylene (PTFE) as binder, this mixture was kneaded and pressed, thus obtaining disc-shaped AC electrodes (with an approximate weight of 30 mg, a diameter of 12 mm and a thickness of approximately 0.4 mm). Symmetric cells were assembled in a two-three electrode configuration (using a sealed T-shaped Swagelok© cell), employing silver wire as pseudo-reference electrode in all the studied cells, glass fiber as separator and gold current collectors (Fig. 1). No springs were used in the cell. All the devices were built in an Ar-filled dry box.

All the electrochemical measurements were performed on a BioLogic VMP Multichannel Potenciostat/Galvanostat at room temperature. The electrochemical behavior of all the EDLC cells were characterized using synchronous galvanostatic charge/discharge cycling test (GCPL), where the cell voltage profiles (identifying the maximum cell voltage) and potential evolution of each electrode (thus determining, at the same time, P^+ and P^-) were simultaneously recorded at different cell voltages (successively from 1 to 3 V) and at a specific current of 50 mA g^{-1}. After the cells were tested at 3 V a new galvanostatic experiment was performed at 1 V to check permanent changes in the electrode. These experiments were noted as 1V_2.

Two cells were measured for each electrolyte to be sure that the behavior was consistent and reproducible (furthermore, also to guarantee the stability of the pseudo-reference electrode used). The determination of P^+ and P^- was done for each voltage as described in Fig. 2 (in this case it is shown the experiment at 1 V).

The capacitance (C), specific energy (E), energy efficiency ($\mathcal{E}$e), coulombic efficiency (η) and equivalent series resistance (ESR) for the cell and each electrode were determined at each cell voltage, as described elsewhere.[22,23] For each voltage and after the synchronous galvanostatic charge/discharge cycling tests, electrochemical impedance spectroscopy (PEIS) measurements were performed on the cell in a two-electrode configuration (both at the OCV and the maximum voltage applied) and separately for the positive and negative electrode (at the maximum potential achieved in each charge/discharge profile (P+ and P−) and also at the OCP) in a three-electrode configuration (see Fig. 2). All the impedance measurements were carried out in the frequency range of 10 mHz to 100 kHz with an alternating potential amplitude of 5 mV, in order

to monitor the evolution of the cell resistance and each electrode resistance when the cell voltage increases.

Summarizing, the full sequence of experiments followed with each electrolyte was:

1. Determination of ZIR of the positive electrode
2. Determination of ZIR of the cell
3. Determination of the OCV of the cell
4. EIS of the cell at the OCV
5. Synchronous GCPL (determining, at the same time, the maximum cell voltage and the P^+ and P^- values) at 0.05 A g-1 up to 1 V (5 cycles) followed by:

   • PEIS of the positive electrode at previously determined P^+ (3 cycles)
   • EIS of the positive electrode at the OCP (3 cycles)
   • PEIS of the negative electrode at previously determined P^- (3 cycles)
   • EIS of the negative electrode at the OCP (3 cycles)
   • PEIS of the cell at 1 V (3 cycles)
   • PEIS of the cell at 0 V (3 cycles)
6. Synchronous GCPL (determining, at the same time, the maximum cell voltage and the P^+ and P^- values) at 0.05 A g^{-1} up to 2 V (5 cycles) followed by:
   • PEIS of the positive electrode at previously determined P^+ (3 cycles)
   • EIS of the positive electrode at the OCP (3 cycles)
   • PEIS of the negative electrode at previously determined P^- (3 cycles)
   • EIS of the negative electrode at the OCP (3 cycles)
   • PEIS of the cell at 2 V (three cycles)
   • PEIS of the cell at 0 V (3 cycles)
7. Synchronous GCPL (determining, at the same time, the maximum cell voltage and the P^+ and P^- values) at 0.05 A g^{-1} up to of 3 V (5 cycles) followed by:
   • PEIS of the positive electrode at previously determined P^+ (3 cycles)
   • EIS of the positive electrode at the OCP (3cycles)
   • PEIS of the negative electrode at P^- (3 cycles)
   • EIS of the negative electrode at the OCP (3 cycles)
   • PEIS of the cell at 3 V (3 cycles)
   • PEIS of the cell at 0 V (3 cycles)
8. Synchronous GCPL (determining, at the same time, the maximum cell voltage and the P^+ and P^- values) at 0.05 A g^{-1} up to 1 V (5 cycles) followed by:
   • EIS of the positive electrode at previously determined P^+ (3 cycles)
   • EIS of the positive electrode at the OCP (3 cycles)
   • PEIS of the negative electrode at P^- (3 cycles)
   • EIS of the negative electrode at the OCP (3cycles)
   • PEIS of the cell at 1 V (3 cycles)
   • PEIS of the cell at 0 V (3 cycles)

Results and Discussion

Textural properties of the electrode material.—The activated carbon used in this study consists of a mesophase pitch chemically activated with potassium hydroxide by using a weight ratio of potassium hydroxide to mesophase pitch equal to 3:1. Figure 3a shows its corresponding N_2 adsorption isotherm. It presents a Type I (a) isotherm, characteristic of an almost exclusively microporous carbon. This is corroborated by the pore size distribution (PSD) in Fig. 3b, which displays almost no pores above 2 nm. Indeed, the activated carbon presents a relatively narrow PSD with two maxima centered at 0.79 and 1.2 nm. The main textural parameters of the carbon material calculated from the isotherm are listed in Table I. It is a highly porous material, with the value of specific surface area above 2000 $m^2\ g^{-1}$, approximately half of this value corresponding to pores smaller than 0.7 nm. Considering the size of the ions making up the electrolytes here analyzed (EMImTFSI and $EMImBF_4$, see Fig. 4) and based on several studies about pore accessibility, pores smaller than 0.7 nm would be poorly accessible to some of the ions, specifically $EMIm^+$ and $TFSI^-$.[24,25] In this way, the accessible area to those ions is reduced to around 900 $m^2\ g^{-1}$ (see Table I), whereas the anion BF_4^- can access all the porosity. The total pore volume is close to 1 $cm^3\ g^{-1}$, with 91% of the total pore volume arising from micropores, confirming its mainly microporous nature (Fig. 3c).

The two ILs chosen for this study share the same cation, but have an anion with different size, which surely affects their performance as electrolyte in the supercapacitor. The smaller size of BF_4^- compared to $TFSI^-$ affects some relevant properties of the electrolyte such as the density (1.28 *vs* 1.52 g cm^{-3}, respectively), the viscosity (25.2 *vs* 35.6 cP at room temperature, respectively) and the electrical conductivity (16.3 vs 9 mS cm^{-1} at room temperature, respectively). All these properties suggest that $EMImBF_4$ should have a better electrochemical response than EMImTFSI, but the strong interactions between cation and anion and between the ions and the surface might change this presumption.

Galvanostatic charge/discharge studies.— *Electrochemical behavior of symmetric EDLCs.*—The electrochemical parameters of the supercapacitors assembled with the activated carbon under study in the two electrolytes are summarized in Table II. The cells were studied at increasing voltage (1, 2 and 3 V) pursuing to understand their behavior. As defined in the experimental section, after the experiments at 3 V, the cell was tested again at 1 V (experiment 1 V_2) to check if the cell suffered any degradation. The corresponding charge/discharge plots are shown in Figs. S1 and S2 in Supporting Information.

For an ideal EDLC, the capacitance is expected to show an independent value vs voltage. However, as can be seen from the data in Table II, the ideal behavior is not followed for any of the ILs. For EMImBF4, with smaller anion size, the maximum specific capacitance is reached at 2 V, while it is necessary to reach 3 V in EMImTFSI to obtain the maximum C, showing the relevance that the electric field has to push the ions deep into certain range of pore sizes. From these results, it is clear that the increase in voltage helps to form the double layer into the narrowest pores that are not naturally filled with the electrolyte. The smallest ions of EMImBF4 needs lower voltages to reach the smallest pores, while higher voltages are required for the larger ions of EMImTFSI. Apart from this fact, the values obtained for both ILs are quite similar at 3 V, getting a specific cell capacitance of 37 F g^{-1}, a specific energy close to 46 Wh kg^{-1}, an energy efficiency of around 65% and a coulombic efficiency of 89%. It is relevant that this last parameter is much higher at lower voltages, which indicates that at 3 V some kind of irreversible reactions start to occur in both electrolytes. The only parameter that presents significant differences for both electrolytes is the cell equivalent series resistance (ESR), which reaches higher values for EMImTFSI than for $EMImBF_4$. In a first approximation, the ions size can explain this behavior, although stability of the IL could also influence this parameter, especially at high voltages. Of course, other parameters like the lower viscosity and the higher ionic conductivity of EMImBF4 (see above) have influence on this behavior.

As a control experiment, the cells were tested again at 1 V after being tested at 3 V (1V_2) to analyze if the cells suffer damage at this high voltage and, as deduced from Table II, they clearly do. The cell capacitance (and consequently specific energy) experiences a significant decrease of 27% in $EMImBF_4$ and 36% in EMImTFSI. Also, the value of ESR is greatly affected, with an important increase, which is again more severe in EMImTFSI. There is also a significant drop in energy efficiency in EMImTFSI that is not observed in $EMImBF_4$.

To get a better understanding of the interactions between the carbon surface and the electrolyte ions, a separate study of the

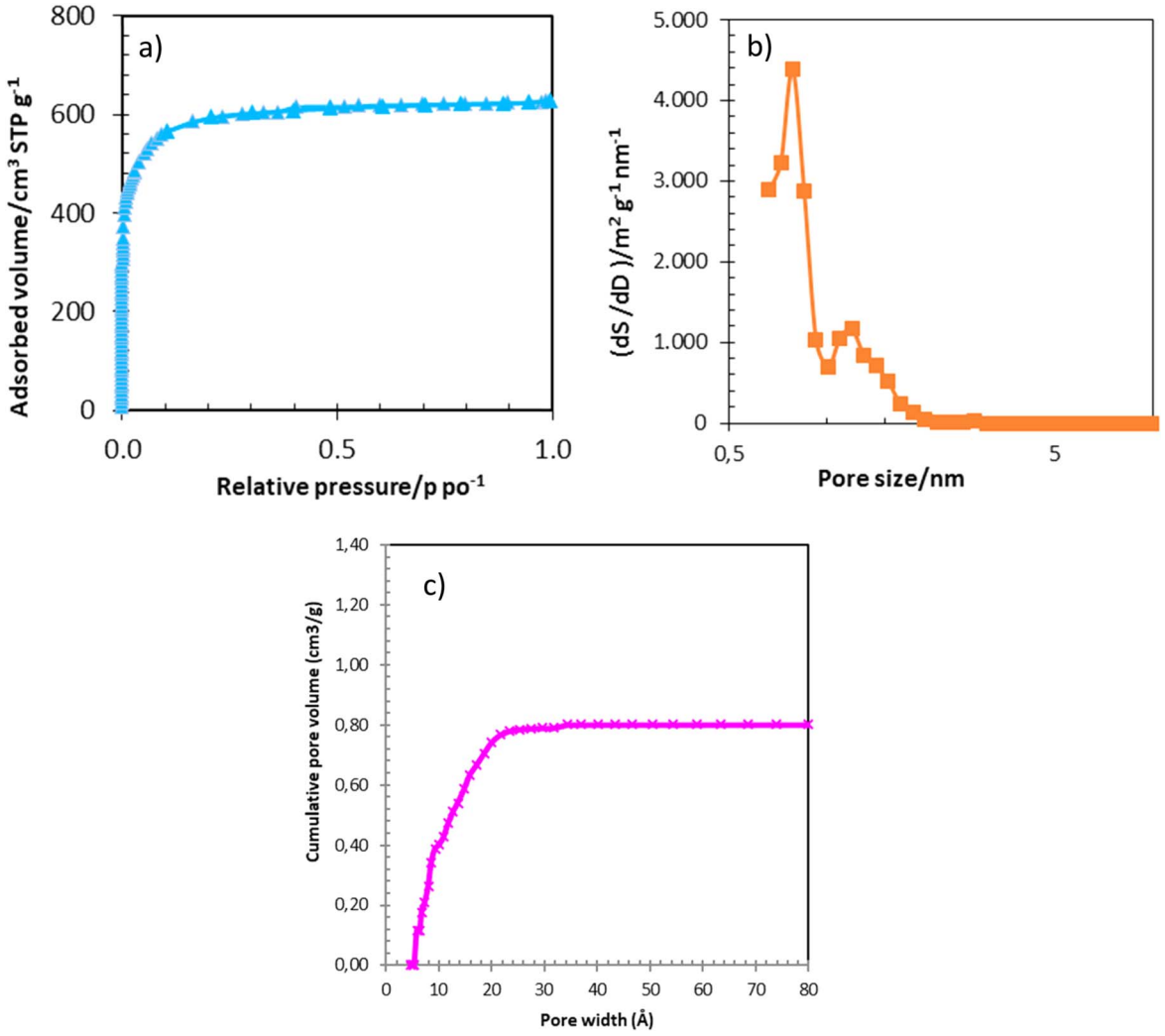

Figure 3. (a) N_2 isotherm at −196 °C, (b) QSDFT pore size distribution and (c) cumulative PSD plot for AC3:1.

Table I. Textural parameters of the carbon material used as electrode.

	AC3:1
BET SSA/m^2 g^{-1}	2292
QSDFT SSA/m^2 g^{-1}	2022
QSDFT SSA pores > 0.7 nm	934
Total pore volume/cm^3 g^{-1} a)	0.89
Micropore volume/cm^3 g^{-1} b)	0.88
Average pore size (per volume)/nm	1.01
Average pore size (D-R)/nm	1.10

a) Determined at a P/Po of ∼0.95. b) Volume of pores <2 nm, determined by using the QSDFT PSD.

behavior of the positive and negative electrodes is shown in the next section.

Electrochemical behavior of the positive and negative electrodes in the symmetric EDLCs.—A more detailed analysis of the systems can be made by studying separately the behavior of the positive and negative electrodes for each cell, as the overlapping of the behavior of both electrodes in the two-electrode system may hide important information. Table III shows the corresponding electrochemical parameters for positive and negative electrodes, which have been determined from the potential profiles in Figs. S1-S2.

Looking at the evolution of specific capacitance with cell voltage for both electrodes, it is clear that, although theoretically the systems are built as symmetric cells, they do not behave with such symmetry, as the results for positive and negative electrolytes are quite different. The asymmetry of the anion and cation sizes of this electrolyte could provide an easy explanation for this fact, but other factors like the forces involved in the equilibrium of the system might also have a strong influence. Looking at the specific capacitance values, it can be concluded that the smaller the ion, the higher the capacitance, as demonstrated by the results obtained in the positive electrode for the anion BF_4^- compared with $TFSI^-$, although these differences are decreasing when voltage is increased. Also worth noting is that the specific capacitance of the negative electrode differs in both ILs (although to a lesser extent that in the positive electrode) despite the fact that the same cation is being adsorbed, i.e. $EMIm^+$. This suggests that the double-layer in the negative electrode is not exclusively populated by the positive counter-ions, but there are also some negative co-ions involved in the process. This result agrees with previous theoretical studies on ILs over electrodes in the presence[28,29] or absence of polarization.[25,28,29] We would like to draw the attention to the large specific capacitance displayed by the positive electrode in both ILs at 3 V, around 180 F g^{-1}, the negative electrode limiting thereby the specific capacitance of the cell.

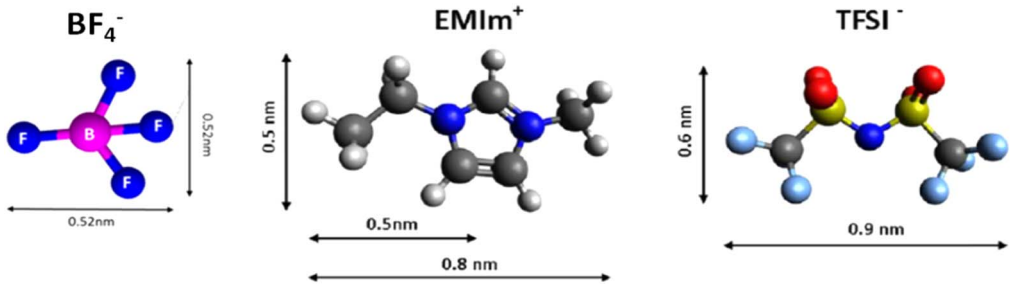

Figure 4. Cation and anion sizes of the ILs employed in this study.

Table II. Electrochemical cell parameters of the supercapacitors assembled with AC3:1 and both ILs.

$EMImBF_4$	C_{cell}/F g^{-1}	E_{cell}/Wh kg^{-1}	$\mathcal{E}_e$/%	ESR cell/Ω	η /%
1 V	29.3	4.1	74	13.1	99
2 V	38.9	21.6	76	8.9	94
3 V	37.5	46.8	66	16.2	89
1 V_2	21.4	3.0	71	18.9	101
EMImTFSI	**C_{cell}/F g^{-1}**	**E_{cell}/Wh kg^{-1}**	**$\mathcal{E}_e$/%**	**ESR cell/Ω**	**η /%**
1 V	27.5	3.8	74	8.6	98
2 V	31.3	17.4	72	18.1	97
3 V	37.2	46.5	64	24.7	89
1 V_2	17.5	2.4	59	33.0	102

Table III. Electrochemical parameters for each electrode (positive and negative).

$EMImBF_4$—E^+	C_{E^+}/F g^{-1}	E_{E^+}/Wh kg^{-1}	$\mathcal{E}_e$/%	ESR E^+/Ω
1 V	131	4	82	4.1
2 V	162	19.7	75	4.4
3 V	185	40	67	7.5
1 V_2	137	2.1	80	8.9
$EMImBF_4$—E^-	**C_{E^-}/F g^{-1}**	**E_{E^-}/Wh kg^{-1}**	**$\mathcal{E}_e$/%**	**ESR E^-/Ω**
1 V	106	4.3	68	9.2
2 V	150	23.6	77	4.5
3 V	127	54.3	67	8.7
1 V_2	62	3.9	67	10.0
EMImTFSI—E^+	**C_{E^+}/F g^{-1}**	**E_{E^+}/Wh kg^{-1}**	**$\mathcal{E}_e$/%**	**ESR E^+/Ω**
1 V	107	3.5	67	6.4
2 V	125	15.8	66	13.1
3 V	176	37.5	63	12.8
1 V_2	106	1.6	58	17.7
EMImTFSI—E^-	**C_{E^-}/F g^{-1}**	**E_{E^-}/Wh kg^{-1}**	**$\mathcal{E}_e$/%**	**ESR E^-/Ω**
1 V	112	4.1	81	2.3
2 V	125	19	78	4.9
3 V	130	56.1	67	11.8
1 V_2	52	3.3	59	15.4

The analysis of the ESR and the $\mathcal{E}e$ also yields some interesting results. For example, in the positive electrode, the resistance is higher when the double-layer is formed by $TFSI^-$ than BF_4^-, probably due to size effects. In the negative electrode, the same cation is forming the double-layer with both electrolytes; however, the values of ESR differ, which indicates that, similarly to the capacitance values, co-ions also play a role in the double-layer formation. Thereby, the ESR is higher in the negative electrode in $EMImTFSI$ than in $EMImBF_4$, similarly to the positive electrode. Only at very low voltages the ESR is strikingly higher for $EMImBF_4$, a fact that is difficult to explain, but it might be expected that different mechanisms of energy storage are involved, including the chemical interaction of the ions with the carbon surface, the electrostatic forces and the ion-ion interactions.[30] On the other hand, the increase of ESR causes a substantial loss of energy efficiency.

The control experiment performed at 1 V after the experiment at 3 V (1V_2) also yields interesting results. Both electrodes in both cells clearly suffer an important degradation, but it is especially important in the negative ones (>50% loss in capacitance), indicating that the degradation of $EMIm^+$ on the electrode surface is the main limitation for the cell voltage. It is also worth mentioning that the ESR remains very high in these experiments, even higher than the ESR obtained at 3 V, indicating that there are permanent changes in the structure of the carbons. In this regard, the increase in ESR is systematically higher in the case of EMImTFSI than $EMImBF_4$ (30%-40% vs < 20% respectively). At 3 V the value of ESR is influenced by the presence of several different phenomena, related with double-layer formation and the presence of undesired side reactions. However, at 1 V only double-layer formation is supposed to occur, and the high resistance can only be due to changes in the electrode surface. In this sense, it has been previously shown that the decomposition of the electrolyte at high voltages can lead to the formation of a SEI layer on the electrode surface.[31] This SEI layer can explain both the increase of ESR and the drop of capacitance due to blockage of the porosity. To ascertain the formation of some passivation layer, a post-mortem analysis by SEM was performed on the electrodes of the $EMImBF_4$ based supercapacitor (Fig. S3, Supporting Information). Previously, the electrodes were thoroughly washed with acetonitrile to eliminate the IL. Table IV shows the F content (at %) for the different electrodes after cycling at 1 and 3 V. The pristine electrode contains 2.9% of F atoms due to the binder used. The electrodes cycled at 1 V contain a similar amount of F since, as expected, at this very low voltage no solid deposits are formed. On the other hand, it can be clearly seen that the F content in the negative electrode after the 3 V experiment is considerably higher (12.5 at %) than that of the electrodes at 1 V and that of the positive electrode after the 3 V experiment, which would confirm the decomposition of the electrolyte at the negative electrode.

Table IV. F content and BET specific surface area of AC3:1 after post-mortem analysis of electrodes cycled in $EMImBF_4$.

	(F, at %)	(S_{BET}, $m^2\ g^{-1}$)[a)]
Pristine electrode	2.9	1943
E^+ at 1 V	2.9	1452
E^- at 1 V	2.5	1473
E^+ at 3 V	2.7	1478
E^- at 3 V	12.5	1131

a) The value of specific surface area is the average of two electrodes of each type, as the experiment was repeated twice to avoid experimental errors.

Post-mortem N_2 adsorption experiments further corroborate the formation of a passivation layer at the negative electrode at 3 V, as deduced from the reduction of the accessible specific surface area ($\sim$ 1130 $m^2\ g^{-1}$) compared to both electrodes at 1 V and the positive electrode at 3 V ($\sim$1450–1470 m^2/g). In addition, the reduction of the accessible area from $\sim$ 1900 $m^2\ g^{-1}$ for the pristine electrode to $\sim$1450–1470 $m^2\ g^{-1}$ for the electrodes after being cycled at 1 V is probably due to the adsorption of some IL molecules inside the porosity of the AC that cannot be easily removed.

To further confirm that the cells were unstable at higher voltages, additional charge/discharge cycling tests were performed using the 2–3 electrode cells at 3.5 and 4.0 V in order to record the working potential window of each electrode. Following these experiments, CVs were performed on each electrode (in the 2–3 electrode cell) using their corresponding working potential window. As can be seen in Fig. S4, the negative electrode experiences a decrease in its capacitance with increasing cell voltage, which leads to an enlargement of its working potential window -since charge balance between electrodes must be kept- and the displacement of its lower working potential to very negative potentials. This accelerates the decomposition of the electrolyte, which is more pronounced when $EMImBF_4$ is used as electrolyte.

Electrochemical impedance spectroscopy studies.— *Symmetric EDLCs.*—Electrochemical impedance spectroscopy is a useful technique to analyze electrochemical systems, but the analysis of the results is rather complicated and the interpretation of the physical-chemical phenomena underlying a spectrum is very complex. Following the galvanostatic charge/discharge experiments at each voltage, EIS was performed for the symmetrical cells, carrying out the measurements in the cell totally discharge (0 V) and at the final voltage (1, 2 or 3 V). Afterwards, EIS was separately tested for the positive and negative electrodes, both at the OCP and at the maximum (positive electrode) or minimum (negative electrode) potentials reached in each system for each tested voltage, results which are thoroughly discussed in the following section.

The results obtained for the cells tested at 1 and 2 V show that, for both electrolytes, the behavior is similar when the experiments are performed with the cell fully discharged at 0 V or charged at 1 or 2 V (see Figs. 5a–5b and 6a–6b). At these low voltages, no chemical changes are expected to happen due to the stability of the ILs and that only the formation of the double–layer has to occur.

For the AC3:1-$EMImBF_4$ system, the Nyquist plots in Fig. 5 show a depressed semicircle at high frequencies, followed by a very large diffusion zone. The similarity between the experiments performed at 0 V and 1 or 2 V (Figs 5a–5b) indicates that, with both states of charge, the system behaves similarly and no other processes than the double-layer formation take place. However, at 3 V, several changes are observed (Fig. 5c). On one hand, the initial resistance of the cell increases from approximately 3.5 ohm (measured on the cell after cycling at 1 and 2 V, Figs. 5a and 5b to more than 6 ohms after cycling at 3 V (Fig. 5c), which denotes a change in the interaction of the electrolyte with the electrode surface, and the semicircle enlarges at 0 V, indicating an increased interfacial resistance. Both features suggest the presence/formation of a SEI layer. Besides, when the Nyquist plot is recorded at 3 V, further enlargement of the semicircle is registered, which may be attributed to the superimposition with some redox processes taking place on the electrode surface, which would be responsible for the modification of the cell (*e.g.*, electrolyte decomposition). These processes are irreversible or partially irreversible, as reflected by the lower η recorded at 3 V (Table II). On the other hand, the higher impedance achieved at low frequencies may be explained by the fact that the double-layer forms deeper into the porosity than at 0 V (and also under lower electric fields such as at 1 or 2 V). These changes are permanent, as demonstrated when the cell is tested again at 1 V (i.e., 1 V_2, Fig. 5d). In this experiment, the curves obtained at 1 V and 0 V are again very similar and also analogous to the curve obtained at 0 V in the 3 V experiment. These results further support the formation of a SEI layer on the electrode surface increasing permanently the interfacial resistance.

The results obtained for the AC3:1-EMImTFSI system are rather similar. As can be seen in Figs. 6a–6b, the Nyquist plots obtained at 1 and 2 V are very similar, measured either at the nominal voltage or at OCV. There is a rather small difference in the curve obtained at 2 V that shows a smaller initial resistance, probably from a better wetting of the electrode surface at the larger electrical field. However, at 3 V some dramatic changes are observed again (Fig. 6c). In accordance with the galvanostatic experiments, the produced damage is permanent, as can be observed in the Nyquist plots registered when the voltage is set back to 1 V (i.e., 1 V_2, Fig. 6d), which is very similar to the Nyquist plot registered at 0 V in the 3 V experiment, but not to the Nyquist plots registered initially at 1 V (in accordance with ESR data, Table II).

Impedance behavior of the positive and negative electrodes: Inductance appearance.—The analyses of the EIS tests in the positive and the negative electrodes (at different potentials and charges) (as schematized in Fig. 2) have been performed for both electrolytes in order to get a deeper insight into the physico-chemical processes involved in the charge/discharge of the electrodes. At this point it is important to remember the sequence of experiments described in the experimental section, as each one of the EIS tests involved three cycles, to guarantee the stability of the silver wire used as pseudo-reference electrode. As will be shown, there are important differences between the behavior of the positive and the negative electrodes, differences that depend both on the electrolyte used and the potential applied. These results would point out to different charge storage mechanisms taking place in the positive and the negative electrodes, which agrees with previous theoretical and experimental studies.[26–30]

In the case of $EMImBF_4$, the recorded Nyquist plots reveal that the negative electrode shows higher values of impedance than the positive one at all the potentials tested, reflecting the difficulties to form the double-layer with the larger ion $EMIm^+$. These results agree with the ESR values measured by galvanostatic charge/discharge for the individual electrodes (see Table III). Looking at the plots at 1 V, it is clear that the behavior of the positive (Fig. 7b) and negative electrodes (Fig. 7a) are quite different and they show different features. The Nyquist plot of the negative electrode is more conventional, showing a large depressed semicircle and a long diffusion zone, characteristic of a double-layer capacitor. However, the Nyquist plot of the positive electrode shows a completely different behavior, and not only due to the lower resistance. The most interesting feature is the presence of a semicircle in the negative zone of the imaginary axis, i.e., an inductive loop. This characteristic is rarely seen in an EDLC (until now it has not been described and explained in the literature for an EDLC) and deserves more attention to study its characteristics and its origin. This phenomenon is observed both at the maximum potential, i.e., P^+, and at the OCP of the positive electrode at all the cell voltages tested, and it is not observed in the negative electrode (see Figs. S6,

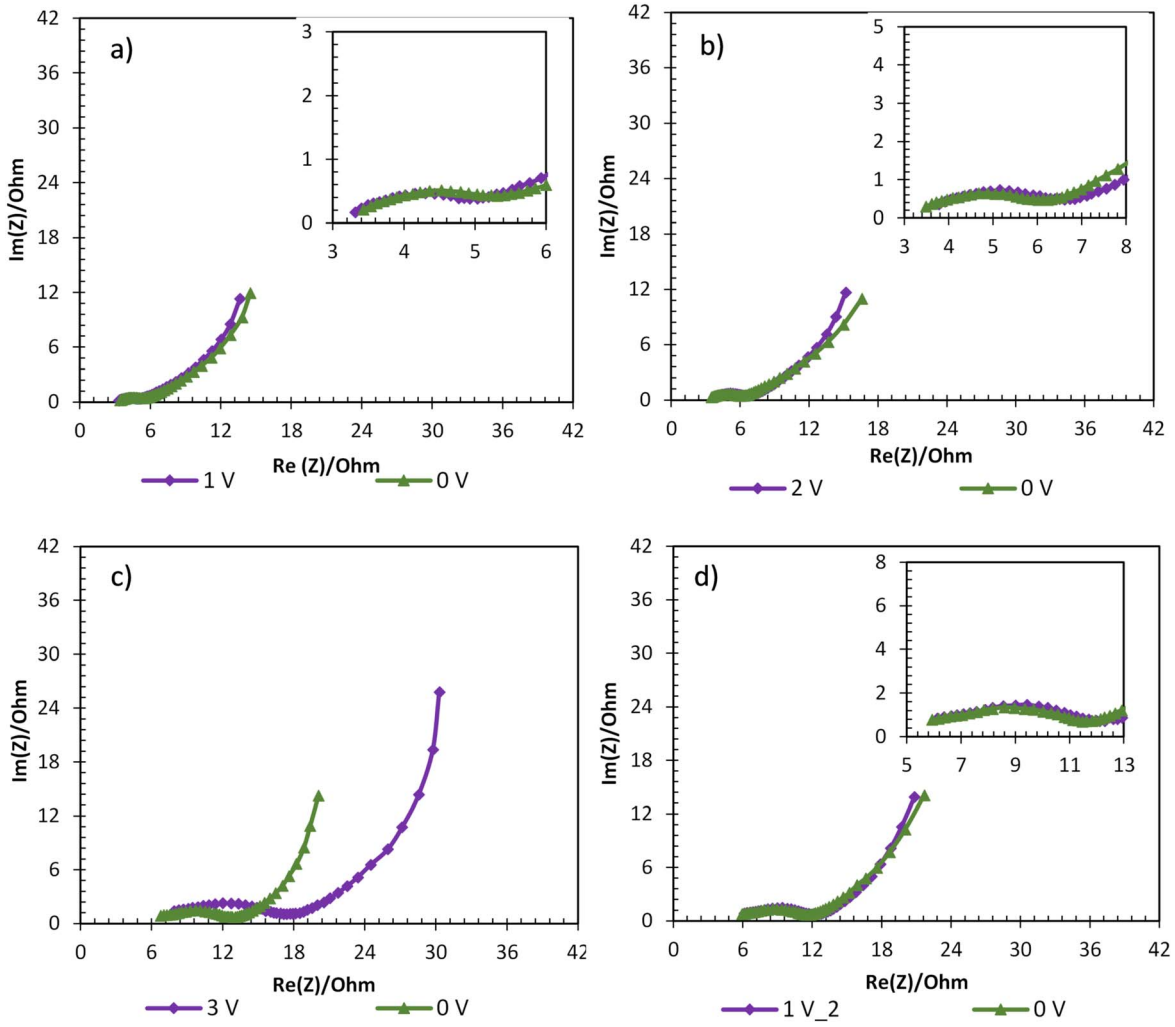

Figure 5. Nyquist plots of the symmetric EDLC based on the AC3:1-EMImBF$_4$ system at different cell voltages: (a) 1 V, (b) 2 V, (c) 3 V and (d) 1 V_2.

S7b, S7d, S8b, S8d, S9b and S9d in SI). Similar results that can be found in the literature in relation to Li-ion batteries have been assigned to artifacts due to the large electrical asymmetry in such systems.[32,33]

These kinds of inductive loops have raised a lot of controversy in the scientific community and no general agreement has yet been achieved about the origin of these signals. Some authors accept that, in the case of lithium batteries anodes, the loop is due to the SEI formation,[31] but others maintain that the loops are artifacts due to the configuration of the experimental devices and the presence of metallic parts in the conventional Swagelok T-cells (like the compression spring and the cylindrical stainless-steel contact).[34] Inductive loops are also encountered in other chemical (due to catalysis, corrosion, electrodeposition), biological (cellular membranes) and material systems (solar cells or OLEDs). An excellent explanation for such phenomena has been given in the literature[35] defining all of them as chemical inductors thus differing from the more traditional electromagnetic inductors. No references have been found for inductive signal in supercapacitors.

To ascertain whether the loops shown in Fig. 7 are due to some real physical processes or are artifacts, some experiments were purposely performed. Besides testing AC3:1 under different experimental conditions (1 to 3 V), other two carbons were tested. One of them is a microporous carbon prepared from citrate (NsC)[36] and the other one is a mesoporous carbon (MC). The textural characteristics of both carbons are shown in Fig. S10, Fig. S11 and Table S1 in SI. The three carbons were electrochemically characterized in the same cells under identical experimental conditions (detailed in the experimental section). Therefore, if the inductive loops were an artifact due to the experimental conditions or to the instability of the silver wire, they should appear with all the carbons.[32–37] Figures S12, S13, S14 and S15 in SI shows the Nyquist plots obtained at different voltages at P^+, P^- and OCP using the three carbon materials as electrodes with the two different ionic liquids as electrolyte. These plots clearly show that the inductive phenomenon in the high frequency region only appear in the systems with microporous carbon electrodes. Thereby, the mesoporous carbon does not present any signal of loops and conventional Nyquist spectra are obtained. Our hypothesis is that the voluminous ions of the ILs confined in the very narrow pores are responsible of the inductive loops, as explained below with more detail.

The different behaviors exhibited by the positive and the negative electrodes are kept at all the experimental conditions tested, so that a single equivalent circuit (EC) can be used to represent the behavior of each of them. Figure 7 also includes the calculated EC for the negative and positive electrodes.

The EC allows calculating the values of the different elements that make up the circuit (Table S2 in SI). Difficulties arise when the elements of the electrical circuit have to be interpreted as physical processes. In the negative electrode, which shows a rather simple and conventional EC for an EDLC, the interpretation is easier. The first part of the EC (R1+R2/Q2) reproduces the formation of the semicircle (Fig. 7a). R1 represents the first point of the curve, and it increases from 1 to 3 V (Table S2 in SI). R1 is normally attributed to

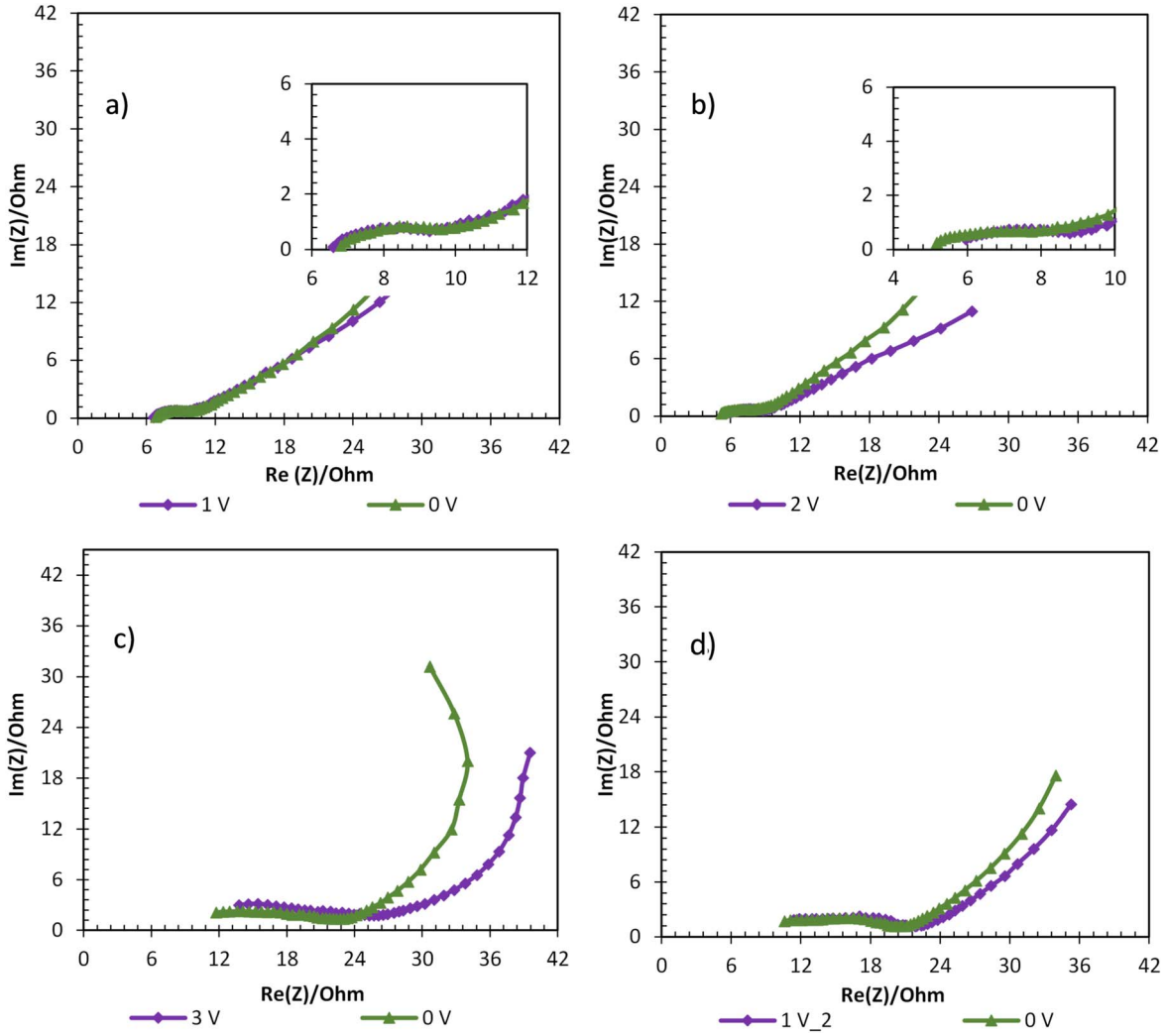

Figure 6. Nyquist plots of the symmetric EDLC based on the AC3:1-EMImTFSI system at different voltages: (a) 1 V, (b) 2 V, (c) 3 V and (d) 1 V_2.

the resistivity of the electrolyte, although it is better to associate it to the resistance of the electrolyte when in contact with the surface of the electrode. The highest value obtained at 3 V is probably due to the modification of the electrode surface, as previously discussed. The element R2/Q2 represents the semicircle and the use of a constant phase element (Q2) instead of a capacitive element (C) is because the semicircle is rather flattened. The values of Q2 are very small due to the high frequencies used, and R2 only reaches very high values at 3 V. At lower frequencies, the element Q3 represents a kind of Warburg element that it is associated with the diffusion of the electrolyte into the porous network. The value of a3 should be 0.5 for a Warburg element, but the experimental values are lower, around 0.3 for all voltages, which represents the difficulties found for diffusion by the highly viscous electrolyte into the micropores network. Finally, the capacitive element C4 represents the double-layer formation at low frequencies. Worth noting are the low capacitance values obtained at 3 V and in the last experiment performed at 1 V (1 V_2), due to the degradation of the electrode when subjecting the negative electrode to a low potential. The drop in capacitance measured in the EIS experiment for the negative electrode and the increase of resistance is in good agreement with the quantitative results shown in Table III for the galvanostatic experiments. The drop in the C values confirms the degradation that the negative electrode suffers when subjecting it to very negative potentials (the positive electrode is more stable).

The positive electrode presents quite a different shape, and it can be fitted to a more complex EC (Fig. 7b). The differences are found in the high frequency zone. Thus, the Nyquist plot presents an inductive loop in combination with different elements, including the characteristic semicircle of the positive *Y*-axis, followed by the negative semicircle mentioned above and a smaller third semicircle that connects with the diffusion zone. As mentioned, the same equivalent circuit has been used to fit the curves obtained for the positive electrode at all voltages and both at P^+ and at OCP. It is found that, apart from R1, three parallel elements are necessary to explain the inductive loop described by the impedance curve in the high to mid frequency region (see inset in Fig. 7b). The inclusion of the capacitive element (C2) implies that a double-layer is forming, probably in the external surface due to the small values of specific capacitance and the high frequencies involved (Table S3 in SI). The constant phase element (Q4) might reflect also double-layer formation, but with some diffusion constraints into porosity. More intriguing is the inductive element (L3) that gives raise to the semicircle in the negative values of the *Y*-axis. The question that arises now is which physical phenomenon underlies the presence of this inductive element in this particular positive electrode that is rarely observed in EDLC. First of all, it has to be mentioned that the detailed experiments performed in this study are not frequently done and that might explain, at least in part, that this fact has not been previously reported.

As shown by several studies, when an IL contacts an electrode, the IL ions (anions and cations) can be adsorbed in the pores of the proper size (excluding the very small pores where the ions cannot fit), unless they are ionophobic (normally because of steric

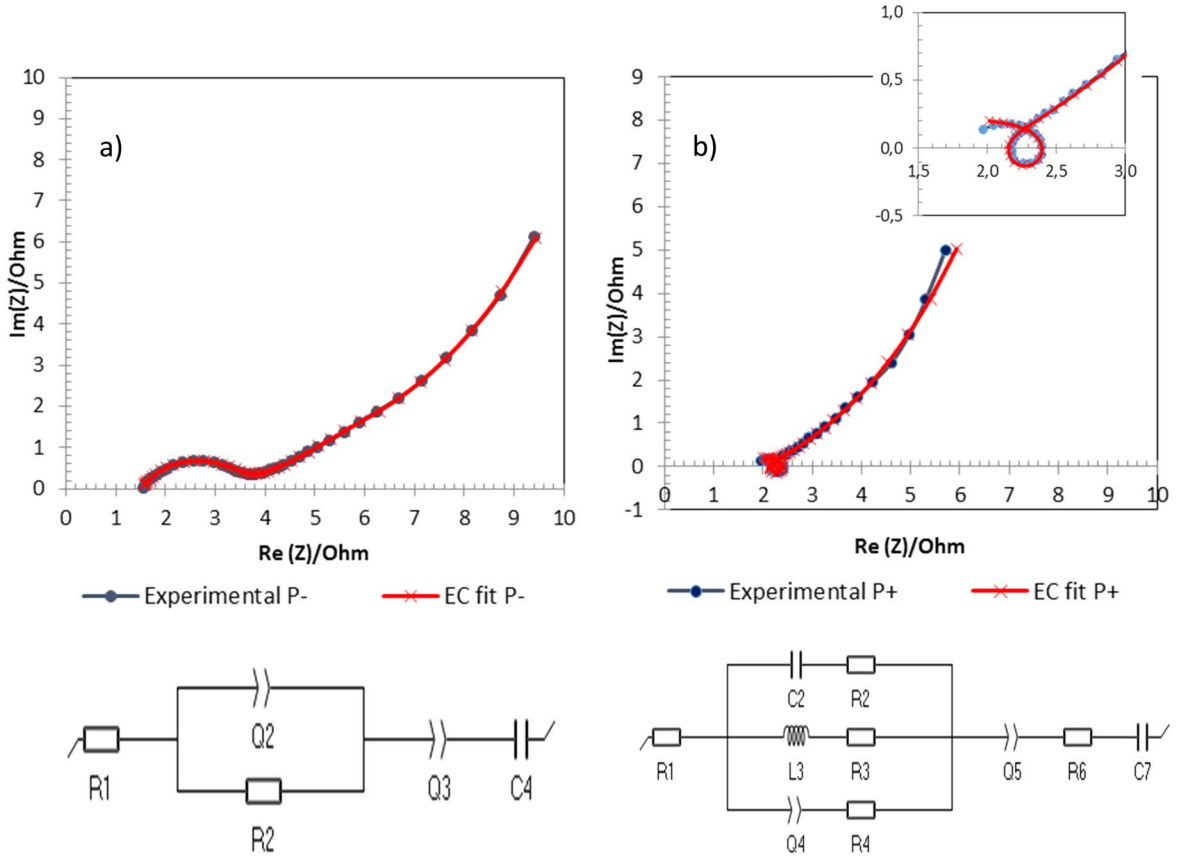

Figure 7. Experimental (blue) and fitted (red) EIS data with the corresponding EC used for the negative (a) and positive (b) electrodes at P^- and P^+ respectively for the AC3:1-EMImBF$_4$ system at 1 V.

effects).[38] When the electrode is polarized, there is a restructuration of the ions on the electrode surface, but this depends on many factors, not only on the electric field. Thus, the interactions of the ions with the carbon surface (confinement effects and surface chemistry) and between themselves have to be taken into account.[27] Figure 8 shows different situations that can occur:

a) Non-polarized pores adsorb a certain number of ions (both positive and negative ones). Of course, the size of the pores determines the adsorption of larger ions. The narrowest pores might not be able to adsorb any ion until the electric field is applied. In an activated carbon like the one used in this study, with a wide distribution of pores sizes (mainly in the micropore range), a heterogeneous behavior might be expected).

b) When the wall of the pores of certain diameter are charged, three charging mechanisms can take place:

1. Counterions (with the opposite charge of the wall) get closer to the wall and the co-ions (with the same charge of the wall) modify their position within the pore.
2. Co-ions desorb from the pore.
3. Co-ions are swapped for counter-ions.

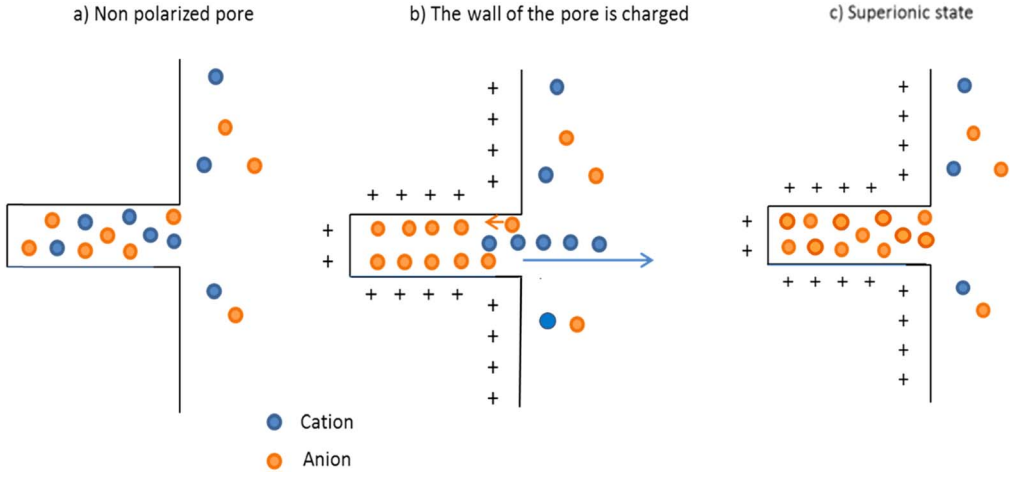

Figure 8. Formation of the superionic state.

c) Under some circumstances, the pore can be enriched in counter-ions and the co-ions can be completely expelled from the pore cavity, reaching the so-called superionic state.

The last two situations create a double-layer, but of course the state described in (c) has higher energy than the state described in b. High electric fields, strong interactions of the counterions with the walls and/or weak interaction between counterions and co-ions favor situation (c). This situation has been described in the literature using different mechanisms, favored when narrow pores are involved. Indeed, when the size of the ions and the pores is similar, there is an exponential screening of the electrostatic interactions between the ions by the charged pore walls, which allows the packing of ions of the same charge, leading to a superionic state.[10,28]

The mechanisms described in Fig. 8 and other similar mechanisms described elsewhere[26–29] can help to understand the physical processes that cause the presence of the inductive elements and that are experimentally detected here. The polarization of the electrode induces the appearance of an electrical current due to the movement of the counter-ions as a result of the electrostatic forces. Meanwhile, the movement of the co-ions out of the pore is the responsible of a countercurrent that is reflected in the EIS spectra as an inductive element. Both, the ion-swapping (as described in Fig. 8) or the co-ions desorption[27,31] could create the signal of the inductive element. The occurrence of ion-swapping on the positive electrode in ILs vs counter-ion adsorption on the negative one has been previously shown by more complex in situ nuclear magnetic resonance and electrochemical quartz crystal microbalance experiments.[39,40] The phenomena above describe might only occur in pores of certain diameters. Larger diameters might not show the ion swapping effect, while smaller diameters are not reachable even at high electric fields. In an activated carbon like the one used in this study, that has a relevant contribution of pores between 0.7 and 2.0 nm, is likely that the three situations take place simultaneously.

As shown in Table III, the charge storage process in the positive electrode is much more energetically efficient (82 vs 68%) and with much lower ESR (4.1 vs 9.2 ohm) than that in the negative electrode. From these results, it is clear that BF_4^- forms the double-layer more easily than $EMIm^+$, which might explain a quick and favored entrance of this ion into the pores with the consequent fast expulsion of the co-ions, which is reflected in the shape of the impedance spectra. It seems that ion-swapping readily occurs in this electrode and it would be dominant even at low potentials. On the contrary, the difficulties to form the double layer of $EMIm^+$ ions in the more resistive negative electrode do not allow the creation of a neat current that can be easily detected.

With regards to EMImTFSI, the system is even more complex and no single EC can be obtained for each electrode, as the EC depends also on the voltage applied. From the results in Table III, it is clear that at 1 V the interaction of $EMIm^+$ ion with the carbon surface is much easier than the interaction of $TFSI^-$ ion, showing lower ESR (2.3 vs 6.4 ohm) and higher energy efficiency (81 vs 67%) when forming the double-layer, probably due to size and/or shape effects. At this voltage (1 V), it is the negative electrode the one that shows peculiar characteristics, such as a new inductive element (see Fig. 9a). It exhibits a vertical zone at very high frequencies, but with negative values of the imaginary component, which can be represented by an inductive element (we will call Type I inductance), followed by a similar semicircle to the one observed in the positive electrode in $EMImBF_4$ (that we will call Type II inductance). Once the curve reaches the positive values of the imaginary axes, it shows almost no semicircle and goes directly into diffusion. The Type I inductance has a very small value of L, two orders of magnitude smaller the Type II inductance (see Table S4 in SI), as obtained from the EC fitting (see Fig. 9a). This kind of inductive element is normally attributed to the wiring and therefore it will not be included in the discussion. The second inductance in the EC, that has a higher value, represents -as occurs in the positive electrode of $EMImBF_4$- the appearance of a countercurrent in the negative electrode, which might be in agreement with ion-swapping or co-ions desorption occurrence. In this case, ions enrichment in the cavity occurs in the negative electrode due to the easier interaction of $EMIm^+$ with the carbon surface that facilitates the removal of the co-ion $TFSI^-$ from the pores. The differences between the inductive element observed in Fig. 7b and Fig. 9a might indicate that the mechanism producing the inductance is different in both electrodes, but more experiments are needed to fully understand these processes and confirm this fact.

In the positive electrode, in the high frequency zone, there is a constant phase element (Q2) that represents the resistance of the electrode to form the double-layer. The diffusion zone at intermediate frequencies, represented by Q3, displays quite different behaviors in the two electrodes. In the positive one, the value of a3 = 0.12 indicates a behavior closer to a resistor than to a capacitor, as shown also by the small slope of the curve (Table S4 in SI). In the negative electrode, the value of a4 = 0.43 is much closer to a Warburg element (a = 0.5) that represents a semi-infinite linear diffusion. At low frequencies, more resistive elements are necessary to explain the behavior of the positive electrode. The competition of $EMIm^+$ with $TFSI^-$ for adsorption sites might be the reason for this behavior and this occurs due to the small electric fields applied.

The Nyquist plots measured at the OCP are very similar to the ones obtained for P^+ and P^- in both electrodes (see Fig. S16 in SI). The small voltage applied, and the small potentials achieved for each electrode at P^+ and P^-, explain this behavior.

At 2 V, the impedance of the negative electrode continues to be smaller than the positive one (in agreement with the charge/discharge experiments, see Table III), but some more changes are observed (Fig. 10a). The positive electrode initial semicircle has grown significantly, along with the highest frequency interception with *X*-axis, and the diffusion impedance is also very large, as denoted by the small slope shown by the linear zone obtained at medium frequencies (Fig. 10b). This large impedance corresponds to the large increase in the ESR in the charge/discharge experiments, which grows from 6 to 13 ohms (see Table III). The negative electrode also experiences an increase of the ESR, but from 2 to 5 ohms (see Table III). The energy efficiencies do not change significantly despite the large ESR variation. As evidenced by Fig. 8a, the most relevant change occurs in the negative electrode with the disappearance of the Type II inductance (the Type I inductance is maintained, but with an even smaller value). Diffusion becomes the main element of the impedance, with a Q4 that is nearly a Warburg element (a4 = 0.51) (Table S5 in SI). This shows that the charge storage mechanism changes from 1 to 2 V in this electrolyte. The experimental evidences seem to indicate that, at 1 V, ion-swapping or co-ions desorption would operate as the main mechanism of energy storage, whereas at 2 V counter-ion adsorption would contribute more to the double-layer formation. With regards to the OCP, there are no significant changes in the Nyquist plots with respect to the ones obtained at P^+ and P^- (see Fig. S17 in SI).

At 3 V, the situation drastically changes and some more complex phenomena occur. For this reason, in addition to the plots obtained at P^+ and P^- (Fig. 11), the plots obtained from the negative and positive electrodes at the OCP are also included in the discussion (Fig. 12). There is a very large increase in the resistance of the negative electrode at P^- with respect to the curve observed at 2 V, with a clear change in the shape of the curve (Fig. 11a). A large semicircle, probably a second small depressed semicircle and the diffusion zones are now present. The first semicircle does not start from a 0 value in the *Y*-axis, but in the positive ones, indicating that, at this large potential, the electrochemical phenomena start at much higher frequencies. The second semicircle at lower frequencies is probably due to chemical reactions taking place on the electrode surface, as it does not appear at the OCP (Fig. 12a). These chemical reactions are responsible for the increase of ESR in the negative electrode (which increases to 11.8 ohm *vs* nearly 5 at 2 V) and the significant decrease of the cell columbic efficiency, which drops below 90% (Table III). It is reasonable to think that in the negative

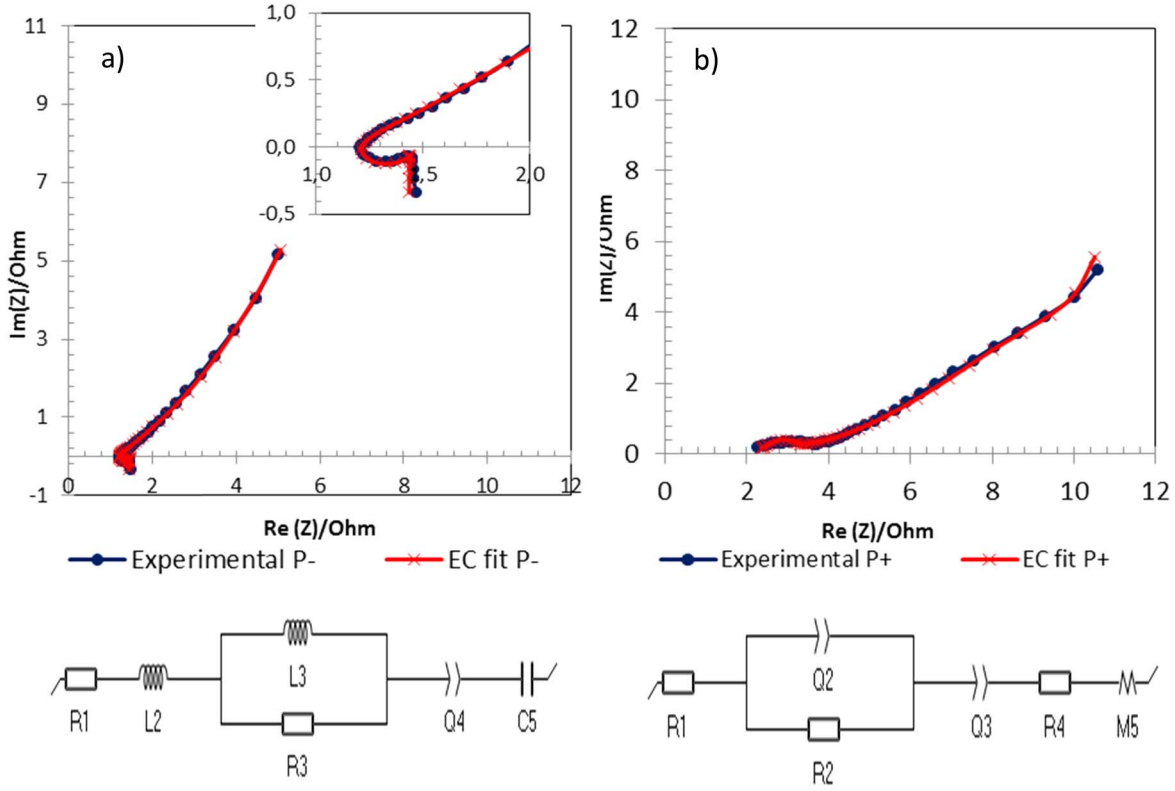

Figure 9. Experimental (blue) and fitted (red) EIS data with the corresponding EC used for the negative (a) and positive (b) electrodes at P^- and P^+ respectively for the AC3:1-EMImTFSI system at 1 V.

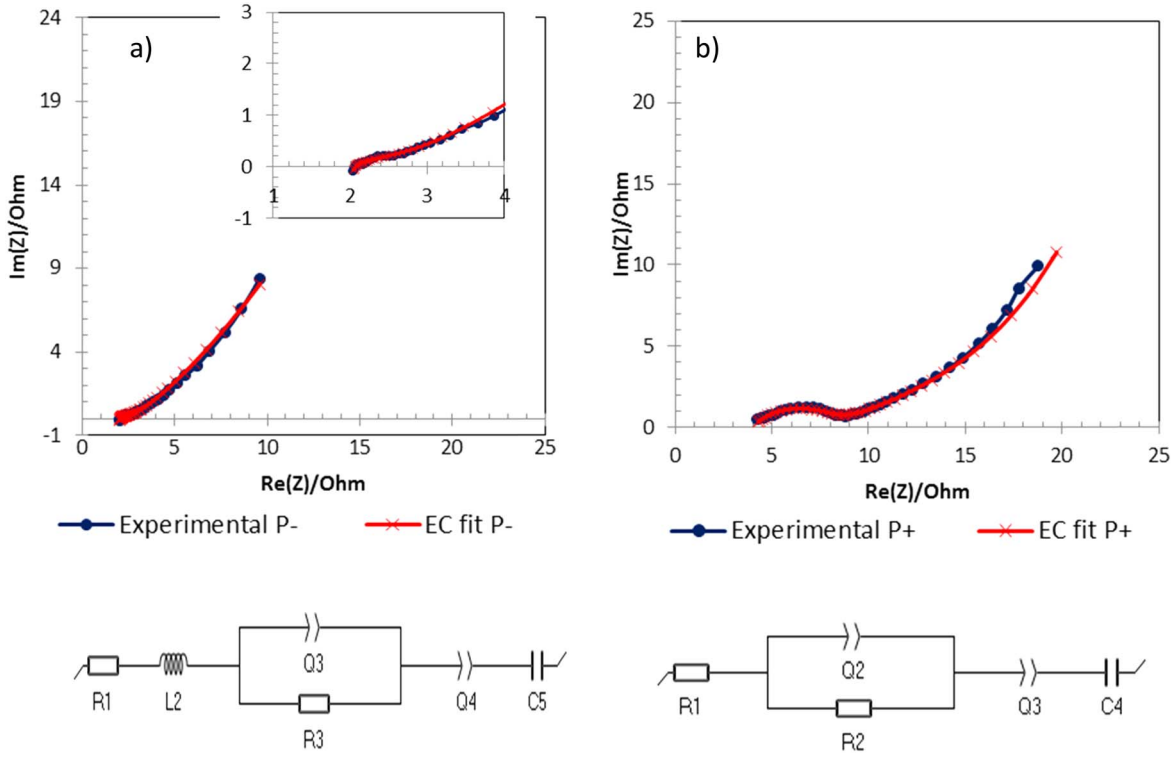

Figure 10. Experimental (blue) and fitted (red) EIS data with the corresponding EC used for the negative (a) and the positive (b) electrodes at P^- and P^+ respectively for the AC3:1-EMImTFSI system at 2 V.

electrode, the chemical reactions occurring at P^- might induce the formation of a SEI layer. Differently to what occurs in a Li-ion anode, this layer would block the access to the pores and would reduce the capacitance in the negative electrode (this phenomenon will be discussed below).

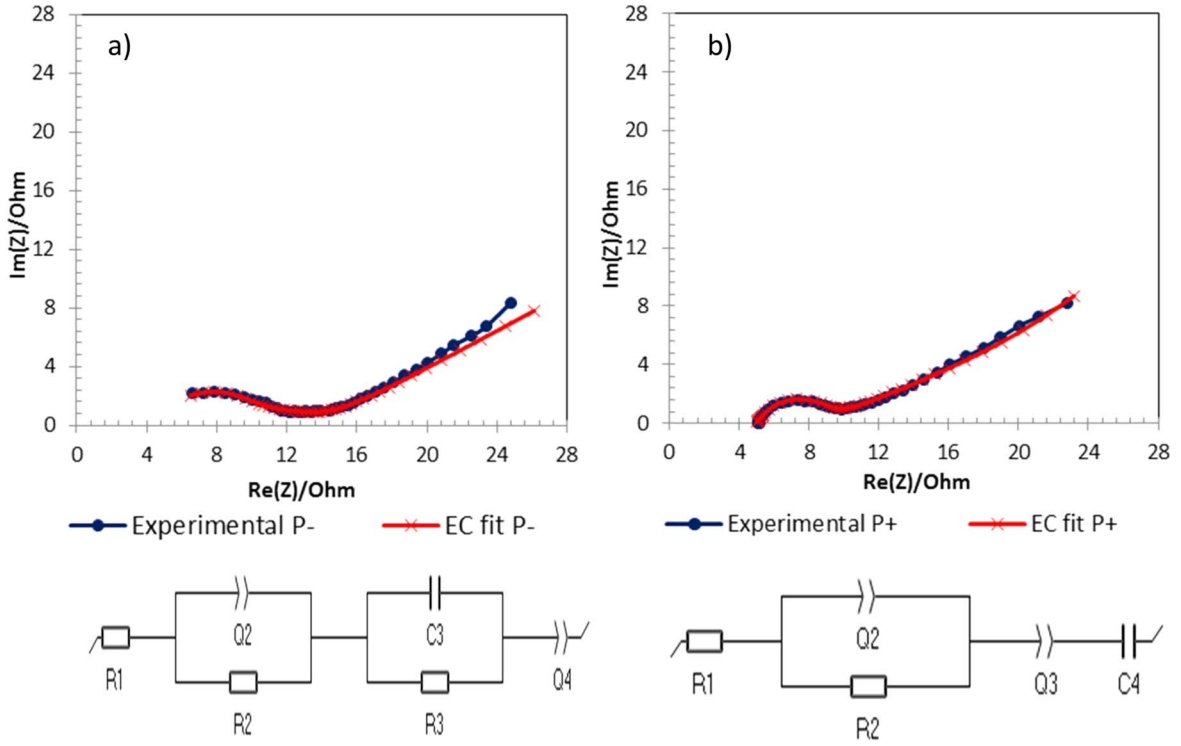

Figure 11. Experimental (blue) and fitted (red) EIS data with the corresponding EC used for the negative (a) and the positive (b) electrodes at the P^- and P^+ respectively for the AC3:1-EMImTFSI system at 3 V.

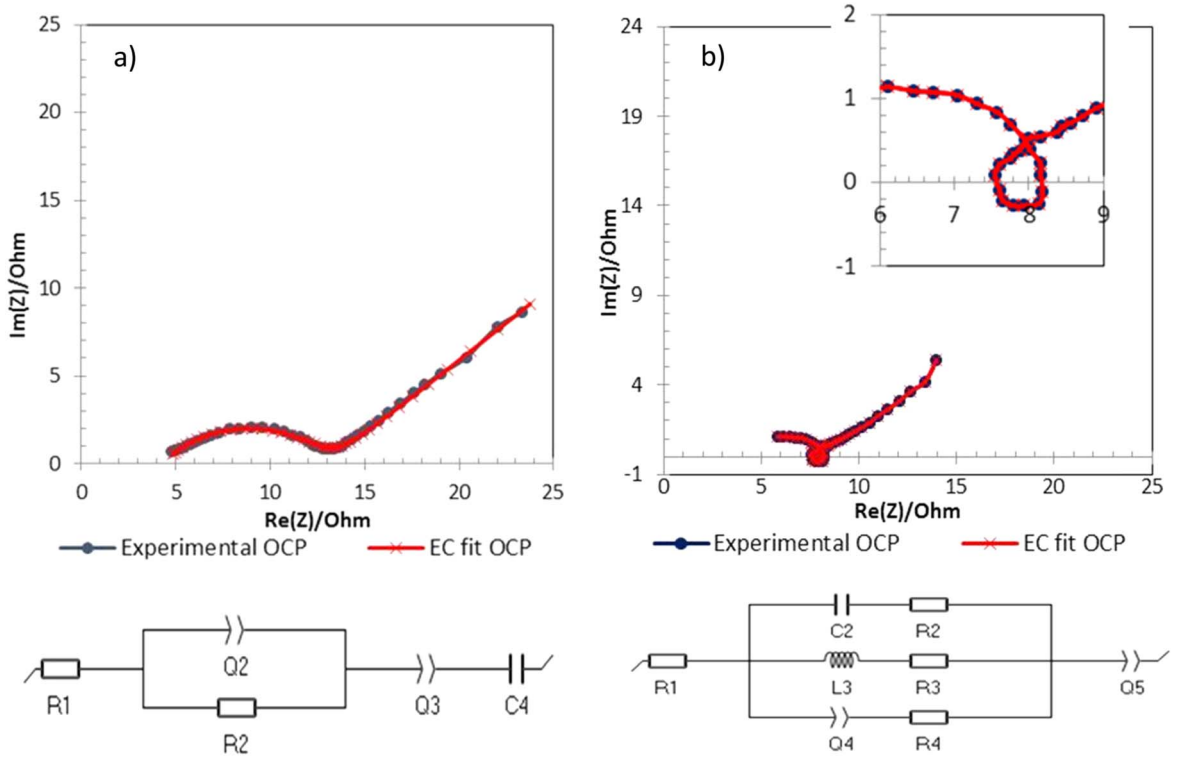

Figure 12. Experimental (blue) and fitted (red) EIS data with the corresponding EC used for the negative (a) and the positive (b) electrodes at OCP respectively for the AC3:1-EMImTFSI system at 3 V.

On the other hand, the positive electrode behaves similarly in P^+ at 2 V (Figs. 10b and 3 V (Fig. 11b), with similar resistances and similar elements in the Nyquist plot, that are the conventional ones (semicircle and diffusion zones). At P^+, the semicircle is represented with an element Q2 that has a2 = 0.83, which means that it is closer to an ideal capacitor, with much smaller resistance (R2 = 3.5 ohms) than the equivalent one in the negative electrode (R2 = 12.3 ohms) (Table S6 in SI). There is no second semicircle, which might

indicate that this positive electrode is more stable than the negative one and the main decomposition reactions occur in the negative electrode. The diffusion elements represent the difficulties for the diffusion of the IL deep into the pores with a low value of a (i.e., 0.28) for Q3.

As previously mentioned, contrarily to what happens at 2 V, the EIS behavior is quite different at the OCP and P^- and P^+ at 3 V. In the negative electrode at the OCP, the second semicircle corresponding to the chemical reactions (Fig. 12a) does not appear, as would be expected for this lower potential, and the experimental curve fits well with the simpler EC. On the other hand, the behavior of the positive electrode at the OCP (Fig. 12b) displays a quite important change with the presence of an inductive element similar to the one discussed for $EMImBF_4$ (with similar EC). The inductive element appears well defined and with a higher value that in previous voltages (see Table S7 in SI). This inductive element that appears at the OCP can be associated with ion-swapping or co-ions desorption. The question that arises is why this element is not observed at P^+. There is not a simple answer to this question and more research is needed to deepen in the understanding of the phenomena that are taking place in the pore system of the electrodes.

After the analysis of the results obtained, many questions arise like, for example, why the inductance appears after the experiment at high voltages with this electrolyte and it appears at lower voltages with $EMImBF_4$, or if the behavior observed for EMImTFSI is due to changes in the electrolyte, the experimental conditions or permanent changes in the carbon structure. In order to get some answers, the cell was studied again at 1 V (experiment named 1 V_2) after the experiment performed at 3 V (see Tables II–III and Fig. 13).

The data in Table II provide some clear indications about the changes of the cell tested at 1 V after being cycled at 3 V with respect to the fresh cell tested at 1 V. The cell shows a significant loss of capacitance, from 27.5 to 17.5 F g^{-1}, showing a clear degradation. This degradation occurs mainly in the negative electrode, which loses more than half of its initial capacitance (from 112 to 56 F g^{-1}), while the positive electrode maintains all of it (from 107 to 106 F g^{-1}), confirming the stability of this electrode (Table III). Furthermore, the negative electrode initially has a very low ESR (*i.e.*, 2.3 Ω) and a very high $\mathcal{E}e$ (*i.e.*, 81%), but after being exposed to 3 V, both parameters become very similar to those of the positive one (17.7 Ω and 58%, respectively), which confirms the accelerated loss of performance. This fact was corroborated with the extra impedance element that was assigned to chemical reactions occurring at the electrode surface, as discussed above.

Figure 13 shows the Nyquist plots for both the negative and the positive electrode at P^- and P^+ respectively in the experiment at 1 V_2. As can be seen in Fig. 13a, the Nyquist plot for the negative electrode at P^- (and also at the OCP, see Fig. S18 in SI) is rather similar to the one obtained at 3 V at the OCP, although a very large semicircle is developed at very high frequencies -probably due to the SEI formation- that is fitted in the EC with a new capacitive element. It is also acceptable to say that it is also rather similar to the original experiment at 1 V (Fig. 7a), but with higher resistance. However, as seen along the discussion, the positive electrode is more changeable with this electrolyte, although in the experiment done at 1 V_2, it maintains the same general shape as in the experiment at 3 V at the OCP, with an even larger inductive element L3 (Table S8 in SI).

The application of 3 V in the system clearly implies decomposition of the electrolyte and permanent changes in the system, with the formation of a SEI layer on the carbon surface (mainly in the negative electrode). The changes occurring in the positive electrode are not so evident, with the capacitance being maintained, but with an important increase in resistance and decrease in energy efficiency. All these changes lead to an increase in the inductance signal, but within these studies, no explanations can be found, and further studies are needed with new carbons (with different pore networks) and probably higher voltages. Attending to the characteristics of the carbon material used in the electrode, it can be easily accepted that, due to the wide pore size distribution, the phenomena detected might not occur in all the surface in the same extension, but only in the pores that have similar sizes to that of the ions (that might be different for positive and negative electrodes), as described in the literature.[30]

It is hard to understand why the inductance associated with the ion-swapping, the superionic state formation or other mechanisms of energy storage, appears in one or the other electrode or in any

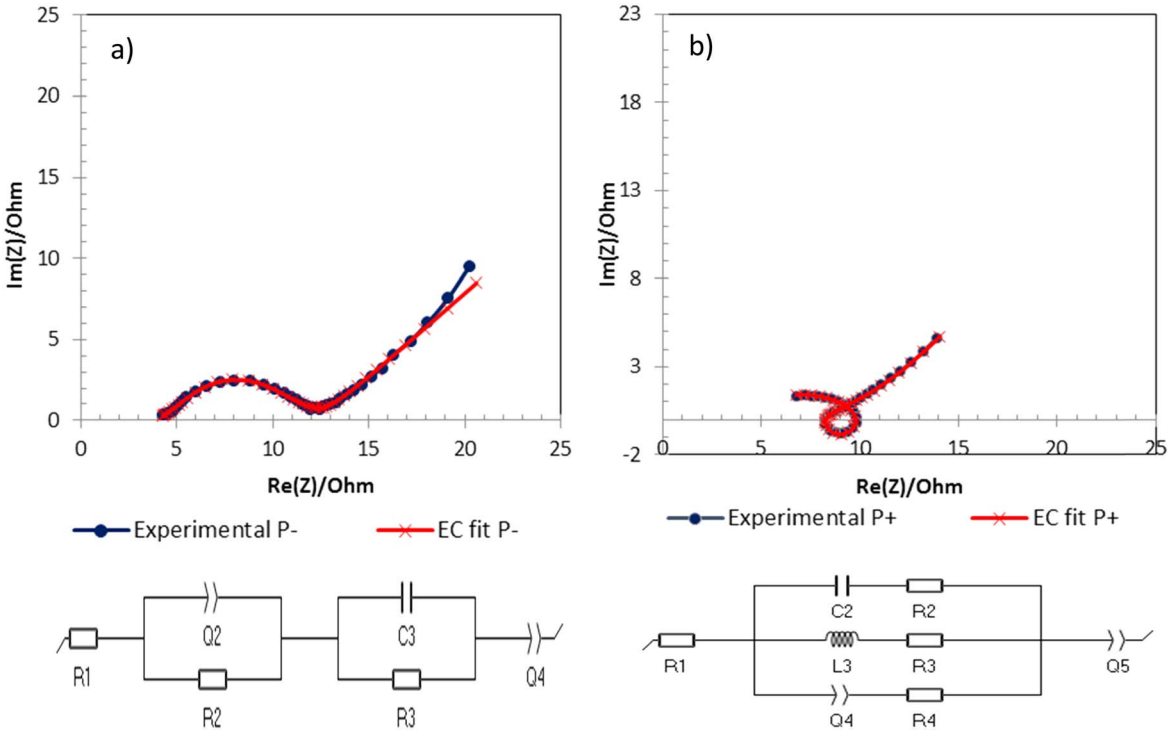

Figure 13. Experimental (blue) and fitted (red) EIS data with the corresponding EC used for the negative (a) and the positive (b) electrodes at P^- and P^+ respectively for the AC3:1-EMImTFSI system at 1 V_2.

particular experimental conditions. It seems to be demonstrated that it appears where the double-layer is specially favored and no other more intense phenomena overlap with the countercurrent produced by ion-swapping, co-ion desorption or the formation of the super-ionic state. It seems also clear from the differences observed between the experiments performed at 1 V and 1 V_2 that the carbon, when subjected to 3 V, undergoes permanent changes that facilitate the inductive effects on the electrodes. It has been proposed elsewhere that this particular kind of activated carbons can show some "flexibility" in the pore walls and that, to a certain extent, they can adjust the pore size to the adsorbate.[41] This might explain that some of the permanent changes that occur in the carbon (beyond the decomposition of the electrolyte on the surface) reinforce the presence of inductive currents, since the existence of pores that yield the maximum interaction with the electrolyte is favored.

Conclusions

The detailed study performed on a microporous carbon-based supercapacitor using two ILs that share the same cation ($EMImBF_4$ and EMImTFSI) has given some very interesting clues to increase our knowledge on the mechanisms involved in energy storage when these unique electrolytes are used. The specific energy achieved with both electrolytes at the maximum voltage tested (3 V) is very similar and high, close to 46 Wh kg^{-1}. There are also evidences that, although it is accepted that these electrolytes are stable at high voltages, degradation of the cells is already detected at 3 V, as reveal by the decrease of the energy and coulombic efficiency, and the increase in cell resistance and the creation of a passivation layer. This degradation mainly occurs in the negative electrode, more markedly in the case of the electrolyte with the $TFSI^-$ anion.

The most relevant results are obtained from the EIS curves performed in the positive and negative electrodes at various potentials. For the first time in supercapacitors, inductive elements are detected in the Nyquist plots and explained. There is no an easy explanation for the physico-chemical processes underlying these signals, but a careful analysis of the data suggests that the counter-currents that generate the inductance signal may be due to ion-swapping or co-ion desorption taking place at least in certain pores with a given diameter, phenomena that have been previously described, but experimental evidences derived from electrochemical measurements have been hardly provided. Depending on the characteristics of the carbon electrodes and of the ions involved, the inductive elements can be present or not, and can be more or less intense, giving indications of the energy storage mechanisms that prevail in each circumstance.

This kind of experiments performed with more electrolytes and different carbon electrodes could bring more experimental evidences on the complex interactions existing between the electrode surface and the ions that compose the ionic liquids.

Acknowledgments

The authors acknowledge Ministerio de Ciencia, Innovación y Universidades for financial support (project MAT2016–77114-R and the predoctoral contract of Noemí Quintanal, BES-2017–082038). Authors would also thank Principado de Asturias (FICYT, Ayudas a grupos de investigación para actividades de I+D+i 2021–2023, AYUD/2021/50249) for its financial support.

ORCID

Ricardo Santamaría https://orcid.org/0000-0001-9818-6998

References

1. B. E. Conway, *Electrochemical Supercapacitors: Scientific Fundamentals and Technological Applications* (New York)(Kluwer Academic Publishers/Plenum Press) (1999).
2. H. Helmholtz, "Studien über elektrische Grenzschichten." *Ann. Phys.*, **7**, 337 (1879).
3. M. Gouy, "Sur la constitution de la charge électrique à la surface d'un électrolyte." *J. Phys. Théor. Appl.*, **9**, 457 (1910).
4. G. Gouy, "Sur la fonction électrocapillaire." *Ann. Phys.*, **9**, 129 (1917).
5. D. L. Chapman, "A contribution to the theory of electrocapillarity." *Philos. Mag.*, **25**, 475 (1913).
6. M. Stern and A. L. Geary, "Electrochemical polarization: A theoretical analysis of the shape of polarization curves." *J. Electrochem. Soc.*, **104**, 56 (1957).
7. C. Vix-Guterl, S. Saadallah, K. Jurewicz, E. Frackowiak, M. Reda, J. Parmentier, J. Patarin, and F. Beguin, "Supercapacitor electrodes from new ordered porous carbon materials obtained by a templating procedure." *Mater. Sci. Eng., B*, **108**, 148 (2004).
8. A. B. Fuertes, G. Lota, T. A. Centeno, and E. Frackowiak, "Dependence of electric double layer capacitance of activated carbons on the types of pores and their surface areas." *Electrochim. Acta*, **50**, 2799 (2005).
9. J. Chmiola, G. Yushin, Y. Gogotsi, C. Portet, and P. Simon, "Anomalous increase in carbon capacitance at pore sizes less than 1 nanometer." *Science*, **313**, 1760 (2006).
10. S. Kondrat, N. Georgi, M. V. Fedorov, and A. A. Kornyshev, "A superionic state in nano-porous double-layer capacitors: insights from Monte Carlo simulations." *Phys. Chem. Chem. Phys.*, **13**, 11359 (2011).
11. R. M. Lynden-Bell, M. G. Del Popolo, T. G. A. Youngs, J. Kohanoff, C. G. Hanke, J. B. Harper, and C. C. Pinilla, "Simulations of ionic liquids, solutions, and surfaces." *Acc. Chem. Res.*, **40**, 1138 (2007).
12. C. Pinilla, M. G. Del Popolo, R. M. Lynden-Bell, and J. Kohanoff, "Structure and Dynamics of a Confined Ionic Liquid. Topics of Relevance to Dye-Sensitized Solar Cells." *J. Phys. Chem. B*, **111**, 4877 (2007).
13. S. K. Reed, O. J. Lanning, and P. A. Madden, "Electrochemical interface between an ionic liquid and a model metallic electrode." *J. Chem. Phys.*, **126**, 084704 (2007).
14. A. Kornyshev, "Double-layer in ionic liquids: paradigm change?" *J. Phis. Chem. B*, **111**, 5545 (2007).
15. M. Alam, M. Islam, T. Okajima, and T. Ohsaka, "Measurements of differential capacitance in room temperature ionic liquid at mercury, glassy carbon and gold electrode interfaces." *Electrochem. Commun.*, **9**, 2370 (2007).
16. M. Sevilla and R. Mokaya, "Energy storage applications of activated carbons: supercapacitors and hydrogen storage." *Energy Environ. Sci.*, **7**, 1250 (2014).
17. A. Alonso, V. Ruiz, C. Blanco, R. Santamaría, M. Granda, R. Menéndez, and S. G. E. de Jager, "Activated carbon produced from Sasol-Lurgi gasifier pitch and its application as electrodes in supercapacitors." *Carbon*, **44**, 441 (2006).
18. D. Lozano-Castelló, D. Cazorla-Amorós, A. Linares-Solano, S. Shiraishi, H. Kurihara, and A. Oya, "Influence of pore structure and surface chemistry on electric double layer capacitance in non-aqueous electrolyte." *Carbon*, **41**, 1765 (2003).
19. E. Frackowiak, K. Jurewicz, S. Delpeux, and F. Beguin, "Nanotubular materials for supercapacitors." *J. Power Sources*, **97–98**, 822 (2001).
20. Y. J. Kim, Y. Horie, Y. Matsuzawa, S. Ozaki, M. Endo, and M. Dresselhaus, "Structural features necessary to obtain a high specific capacitance in electric double layer capacitors." *Carbon*, **42**, 2423 (2004).
21. F. Beguin and E. Frackowiak, *Supercapacitors: Materials, Systems, and Applications* (Germany)(Wiley-VCH Verlag GmbH & Co) (2013).
22. S. Roldán, D. Barreda, R. Menéndez, R. Santamaría, and C. Blanco, "An approach to classification and capacitance expressions in electrochemical capacitors technology." *Phys. Chem. Chem. Phys.*, **17**, 1084 (2015).
23. P. F. R. Ortega, G. A. dos Santos Jr, J. P. C. Trigueiro, G. G. Silva, N. Quintanal, C. Blanco, R. L. Lavall, and R. Santamaría, "Insights on the behavior of imidazolium ionic liquids as electrolytes in carbon-based supercapacitors: an applied electrochemical approach." *J. Phys. Chem. C*, **124**, 15818 (2020).
24. C. Largeot, C. Portet, J. Chmiola, P. L. Taberna, Y. Gogotsi, and P. Simon, "Relation between the ion size and pore size for an electric double-layer capacitor." *J. Am. Chem. Soc.*, **130**, 2730 (2008).
25. R. Futamura, T. Iiyama, Y. Takasaki, Y. Gogotsi, M. J. Biggs, M. Salanne, J. Ségalini, P. Simon, and K. Kaneko, "Nature materials, partial breaking of the coulombic ordering of ionic liquids confined in carbon nanopores." *Nat. Mater.*, **16**, 1225 (2017).
26. W. Peng, J. Huang, V. Meunier, B. G. Sumpter, and R. Qiao, "Voltage dependent charge storage modes and capacity in subnanometer pores." *J. Phys. Chem. Lett.*, **3**, 1732 (2012).
27. J. Vatamanu, M. Vatamanu, and D. Bedrov, "Non-faradaic energy storage by room temperature ionic liquids in nanoporous electrodes." *ACS Nano*, **9**, 5999 (2015).
28. S. Kondrat and A. Kornyshev, "Superionic state in double-layer capacitors with nanoporous electrodes." *J. Phys. Condens. Matter*, **23**, 022201 (2010).
29. S. Kondrat and N. Georgi, "A superionic state in nano-porous double-layer capacitors: insights from monte carlo simulations." *Phys. Chem. Chem. Phys.*, **13**, 11359 (2011).
30. L. Xing, J. Vatamanu, O. Borodin, and D. Bedrov, "On the atomistic nature of capacitance enhancement generated by ionic liquid electrolyte confined in sub-nanometer pores." *J. Phys. Chem. Lett.*, **4**, 132 (2013).
31. K. L. Van, "Aken, relationship between carbon electrode materials and electrolytes in capacitive energy storage." *Doctoral Thesis*, Faculty of Drexel University (2017).
32. M. Ender, A. Weber, and E. Ivers-Tiffée, "Analysis of three-electrode setups for ac-impedance measurements on lithium-ion cells by fem simulations." *J. Electrochem. Soc.*, **159**, A128 (2011).
33. C. Delacourt, P. L. Ridgway, V. Srinivasan, and V. Battaglia, "Measurements and simulations of electrochemical impedance spectroscopy of a three-electrode coin cell design for Li-Ion cell testing." *J. Electrochem. Soc.*, **161**, A1253 (2014).

34. H. Brandstätter, I. Hanzu, and M. Wilkening, "Myth and reality about the origin of inductive loops in impedance spectra of lithium-ion electrodes - a critical experimental approach, materials science." *Electrochim. Acta*, **207**, 218 (2016).
35. J. Bisquert and A. Guerrero, "Chemical Inductor." *J. Am. Chem. Soc.*, **144**, 5996 (2022).
36. A. B. Fuertes and M. Sevilla, "Hierarchical microporous/mesoporous carbon nanosheets for high-performance supercapacitors." *ACS Appl. Mater. Interfaces*, **7**, 4344 (2015).
37. S. B. Adler, "Reference electrode placement in thin solid electrolytes." *J. Electrochem. Soc.*, **149**, E166 (2002).
38. A. C. Forse, C. Merlet, J. M. Griffin, and C. P. Grey, "New perspectives on the charging mechanisms of supercapacitors." *J. Am. Chem. Soc.*, **138**, 5731 (2016).
39. W.-Y. Tsai, P.-L. Taberna, and P. Simon, "Electrochemical quartz crystal microbalance (eqcm) study of ion dynamics in nanoporous carbons." *J. Am. Chem. Soc.*, **13624**, 8722 (2014).
40. J. M. Griffin, A. C. Forse, W.-Y. Tsai, P.-L. Taberna, P. Simon, and C. P. Grey, "In situ NMR and electrochemical quartz crystal microbalance techniques reveal the structure of the electrical double layer in supercapacitors." *Nat. Mater.*, **14**, 812 (2015).
41. D. Barreda et al., "Unusual flexibility of mesophase pitch-derived carbon materials: An approach to the synthesis of graphene." *Carbon*, **115**, 539 (2017).